
Article:
Carcadea, E., Varlam, M., Ismail, M. et al. (6 more authors) (2019) PEM fuel cell performance improvement through numerical optimization of the parameters of the porous layers. International Journal of Hydrogen Energy. ISSN 0360-3199

https://doi.org/10.1016/j.ijhydene.2019.08.219

PEM fuel cell performance improvement through numerical optimization of the parameters of the porous layers

E. Carcadea[a*], M. Varlam[a], M. S. Ismail[b], D.B. Ingham[b], A. Marinoiu[a], M. Raceanu[a], C. Jianu[a], L. Patularu[a] and D. Ion-Ebrasu[a]

[a]National Research and Development Institute for Cryogenics and Isotopic Technologies - ICSI Rm. Valcea, 240050, Romania

[b]Energy2050, Department of Mechanical Engineering, Faculty of Engineering, University of Sheffield, Sheffield S10 2TN, UK

(*) elena.carcadea@icsi.ro

Abstract

A numerical model for a PEM fuel cell has been developed and used to investigate the effect of some of the key parameters of the porous layers of the fuel cell (GDL and MPL) on its performance. The model is comprehensive as it is three-dimensional, multiphase and non-isothermal and it has been well-validated with the experimental data of a 5 cm² active area-fuel cell with/without MPLs. As a result of the reduced mass transport resistance of the gaseous and liquid flow, a better performance was achieved when the GDL thickness was decreased. For the same reason, the fuel cell was shown to be significantly improved with increasing the GDL porosity by a factor of 2 and the consumption of oxygen doubled when increasing the porosity from 0.40 to 0.78. Compared to the conventional constant-porosity GDL, the graded-porosity (gradually decreasing from the flow channel to the catalyst layer) GDL was found to enhance the fuel cell performance and this is due to the better liquid water rejection. The incorporation of a realistic value for the contact resistance between the GDL and the bipolar plate slightly decreases the performance of the fuel cell. Also the results show that the addition of the MPL to the GDL is crucially important as it assists in the humidifying of the electrolyte membrane, thus improving the overall performance of the fuel cell. Finally, realistically increasing the MPL contact angle has led to a positive influence on the fuel cell performance.

Keywords: PEM fuel cell; numerical model; porous layers; graded porosity; sensitivity analysis; performance improvement.

1. Introduction

Polymer electrolyte membrane fuel cells (PEMFCs) have been intensively investigated during the past decade and this is due to their ability to obtain the electrical energy from the chemical energy of a fuel and oxidant. In particular, considerable attention has been given to the components that can influence the performance, life time and durability [1-3]. PEM fuel cells consist of a membrane electrode assembly (MEA) which is sandwiched between bipolar plates (BP), see Fig. 1. The MEA is a five layered structure composed of a polymer electrolyte membrane (PEM) with a catalyst layer (CL) and a gas diffusion layer (GDL) on each side (anode-cathode). Usually, the GDL is coated with a micro-porous layer (MPL) in order to mitigate electrode flooding and the contact resistance between the GDL and the catalyst layer. Further, the channels for supplying the reactants and removing the products are grooved into the bipolar plates.

Considerable efforts have been directed towards finding the best materials [4-6] and configurations [7-9] for the PEMFC layers in order to meet the performance and cost requirements. The parameters, such as porosity, permeability, water contact angle, conductivity, contact resistance and thickness of the porous layers must be considered in order to determine their influence on the PEMFC performance. Therefore, the structural, transport and electrochemical parameters that characterize the PEMFC layers need to be optimized and Computational Fluid Dynamics (CFD) simulations are a necessary step for analysing their effect on the PEMFC performance. In addition to the insight into the phenomena that takes place in the fuel cell at microscopic and macroscopic levels, CFD simulations assist in identifying the limiting parameters and in reducing the time and costs

required for the experiments [10-11]. In this respect, the gas diffusion and micro-porous layers are fundamental components due to their position between the bipolar plate having a macroscopic flow field and the catalyst layer in which the electrochemical reactions occur at the microscopic level and also due to the different roles that these layers perform inside the fuel cell. The GDL plays several roles, namely it allows the effective reactant transport from the gas channels to the catalyst active sites, it provides a pathway for the electrons from the CLs to the BPs, it assists in managing the water in the MEA, it mechanically supports the membrane and CL, and it assists in dissipating excess heat [12-20]. The coating of the GDL with an MPL normally leads to an enhancement in the electrical conductivity [21] and water management [22-24] of the GDL sandwich and this is because of the relatively small pore size and increased hydrophobicity of the MPL. The formation of excess water in the PEMFC is a significant challenge for an adequate operation and for a better performance. Further, the oxygen reduction reaction (ORR) taking place in the cathode side leads to the formation of liquid water which possibly fills the pores in the GDL, thus potentially hindering the reacting gases transport to the catalyst layers and subsequently reducing the performance of the fuel cell.

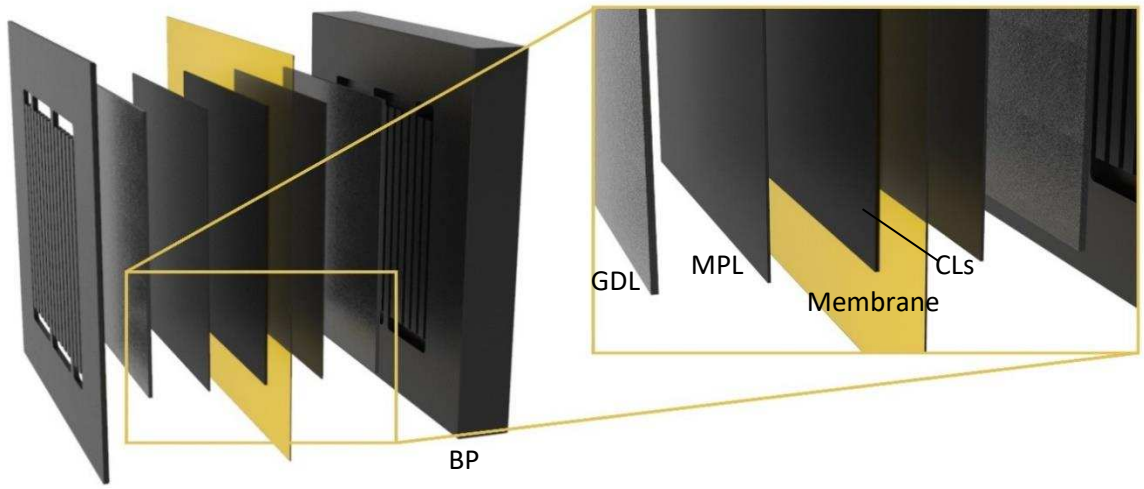

Fig. 1 – Expanded view of the PEM fuel cell components.

The complex interactions between the layers of the PEM fuel cell still requires significant experimental and theoretical investigations. There are a number of studies that have been devoted to developing numerical models for analysing the influence of some of the GDL parameters on the PEMFC performance, namely thickness [13, 25-27], porosity [14-17, 28], permeability [29-32] or contact angle [13, 33-34]. Notably, the porosity of the GDL has a tremendous impact on the performance of the PEM fuel cell. Higher porosity values can lead to a decrease in the water saturation and to an improvement in the performance due to a greater space being available for the reactant gases diffusion and for disposal of the produced liquid water [35-36] and equally it can be detrimental for the electrical conductivity and for the structural support of the other layers (MPL, CL and membrane) [34, 37]. Chun et al. [13] performed an investigation regarding the effect of contact angle, gas permeability and thickness of the GDL on the fuel cell performance and concluded that a thin thickness, high contact angle and high gas permeability are favourable for improving the cell performance, especially at high current densities. Their study involved both numerical analysis and experimental tests.

The GDL properties change when the PEM fuel cell is assembled in a stack due to the compression applied [37-43]. The GDL porosity and other transport properties, including permeability and diffusivity, are relatively low under the rib due to the increased compression. This leads to a smaller oxygen concentration and a higher water saturation in these regions and thus resulting in a decreased fuel cell performance [41]. The contact electrical resistance between the GDL and BP is influenced by the clamping force being applied when assembling the cell layers [42]. A low clamping force leads to an increase of the interfacial electrical resistance and to a possibility of leakage while a high clamping force causes a decrease of the contact resistance but at the same time

reduces the GDL porosity, thus leading to an increased mass transport resistance, especially under the ribs.

One way to reduce the performance loss due to liquid water accumulation is to increase the electrode porosity at the cathode outlet where this excess water accumulates [37] and this can be achieved by using carbon cloth instead of carbon fibre paper or by inserting some holes in the carbon fibre near the oxidant outlet where the flooding occurs. Also, performance loss due to accumulation of liquid water could be diminished if hydrophobic particles are added to the gas diffusion layer or if GDLs with different substrates and variable porosities are used [38, 45]. Taking into account that the manufacturing process of GDLs leads to non-homogeneous materials, it is important to consider a graded porosity, both along the thickness and laterally across the layer. Zhang et al. [5] used the graded porosity concept based on an optimal distribution of the porosity in order to improve the uniformity of the current density along the flow direction and maximise the power density of the fuel cell. In their study, the GDL porosity variation is just along the fluid flow direction in the fuel cell, being a function of the location y, and no in-plane variation of the GDL porosity is taken into account.

There are only a few studies that have analysed the effect of the GDL graded porosity on the water management, gas flow, current density or durability of the fuel cell [5, 12, 14-16, 44-45]. The aim of the gradual decrease in the GDL porosity between the flow channel and the catalyst layer is to provide sufficient reacting gases in the active sites of the catalyst layer, thus leading to uniform electrochemical reaction rates and local current density. A linear porosity variation in the cathode GDL used in the study [16] has led to better water management. Further, an optimal porosity distribution was obtained for two flow field configurations, namely parallel and z-serpentine [16]. Kong et al. [12] experimentally and numerically evaluated the influence of the double gas diffusion layer on the fuel cell performance and self-humidification of the membrane electrolyte. The results showed that an improved water retention capability was obtained by using a double-layered GDL. Another way to obtain a porosity gradient, according to Chen [15], is to add MPLs with different carbon loadings to the surface of the GDL facing both the catalyst layer and the flow field side. This configuration leads to an enhanced oxygen transport through the GDL and to a higher rate of liquid water removal. Also, Tang et al. [44] obtained a graded porosity in the MPL by using different contents of NH_4Cl as pore-former and their results showed a better performance of the PEM fuel cell due to the better transport rates of the liquid water and reacting gases. It is clear from the findings of the above-mentioned investigations that the graded porosity of the GDL has a positive impact on the fuel cell performance.

The present work investigates the consequences of varying some of the key parameters of the GDL and MPL, which are normally considered when manufacturing the latter porous layers, on the PEMFC performance. There are three stages that are essential for the manufacture of the carbon fibre-based GDL, namely electrospinning, stabilizing, and carbonization. The electrospinning techniques were used in our previous work devoted to GDL production and some preliminary results have been obtained [46]. However, an optimum simulated set of parameters, including the fibre diameter, contact angle and porosity would be an advantage and will give a good guide to the operating conditions of the other two experimental steps. The optimum properties of the CL were numerically determined previously [47] and used as inputs in this study. Thereby, the objective of this paper is to optimise the key properties of the GDL and MPL materials using CFD simulations, thus providing much better insights for the manufacture of these porous layers that ensures much better cost-effectiveness and fuel cell performance and durability.

2. Mathematical Model Development

The mathematical model developed in our previous studies [48] for understanding the complex phenomena that occur in fuel cells is based on the mass, momentum, species, charge and energy conservation equations [49-51]. The electrochemical processes are taken into account through the source terms added to these transport equations. The fuel cell operates under steady state conditions and the fuel and air are assumed to be incompressible and laminar. Also, our previous model [47]

took into account the various forms of water, namely gaseous, liquid and dissolved phases and the mass transport resistance due to the catalyst microstructure [52]. For the sake of brevity, the governing equations of the model are not reported in this work as they are available in one of our previous publications [47]. However, for the convenience of readers, some of the relations that are of strong relevance to the analysis of the results of the study are presented.

The existence of three phases in the porous layers of a PEM fuel cell make the modelling of the transport properties a complex task. There is, on one hand, the solid phase present in the porous layers having a complex pore structure that influences the transport of the other two phases, liquid (l) and gaseous (g). On the other hand, the last phases mentioned and the mass transfer mechanism between them requires a comprehensive understanding due to possible interactions and mass exchange.

Assuming laminar and incompressible flow, the fluid flow in a porous media is governed by the Darcy law:

$$u_g = -\frac{KK_r}{\mu_g}\nabla p_g \tag{1}$$

$$u_l = -\frac{KK_r}{\mu_l}\nabla p_l \tag{2}$$

where the effective permeability and the product KK_r take into account each phase and the porous matrix , K (m^2) is the absolute permeability of the medium and it is calculated based using the Carman-Kozeny equation [56] and the dimensionless relative permeability, $K_r\,(-)$, which is approximated by the cube of the phase saturation [57] as shown in Equation (4):

$$K = \frac{\left(\varepsilon^3 d_f^2\right)}{180(1-\varepsilon)^2} \tag{3}$$

$$K_r = \begin{cases} s^3 & for\ liquid\ phase \\ (1-s)^3 & for\ gas\ phase \end{cases} \tag{4}$$

where ε is the porosity, μ is the dynamic viscosity and d_f is the fibre diameter.

The liquid water transport driving force is given by the pressure gradient of the liquid water (∇p_l). The transport equation for the liquid water inside the porous electrodes and membrane takes into account the liquid pressure as a sum of the capillary pressure p_c and gas pressure p, being given by:

$$\nabla \cdot \left(\frac{\rho_l KK_r}{\mu_l}\nabla(p_c + p)\right) = S_{ld} - S_{gl} \tag{5}$$

where ρ_l is the liquid water density, μ_l is the liquid water dynamic viscosity, S_{gl} is the rate of mass change between gas and liquid phases and S_{ld} is the rate of mass change between the liquid and dissolved phases occurring only in the catalyst layers and the membrane:

$$S_{gl} = \begin{cases} \gamma_e \cdot \varepsilon \cdot s \cdot D_{gl} \cdot \frac{M_{H_2O}}{RT} \cdot p \cdot ln\left(\frac{p-p_{sat}}{p-p_{wv}}\right) & p_{wv} \le p_{sat} \\ \gamma_c \cdot \varepsilon \cdot (1-s) \cdot D_{gl} \cdot \frac{M_{H_2O}}{RT} \cdot p \cdot ln\left(\frac{p-p_{sat}}{p-p_{wv}}\right) & p_{wv} > p_{sat} \end{cases} \tag{6}$$

$$S_{ld} = s \cdot \gamma_{ld} \cdot M_{H_2O} \cdot \frac{\rho_i}{EW}\left(\lambda_{eq} - \lambda\right) \tag{7}$$

$$D_{gl} = \begin{cases} 0.365 \cdot 10^{-4} \left(\frac{T}{343}\right)^{2.334} \cdot \left(\frac{10^5}{p}\right) & cathode \\ 1.79 \cdot 10^{-4} \left(\frac{T}{343}\right)^{2.334} \cdot \left(\frac{10^5}{p}\right) & anode \end{cases} \quad (8)$$

$$\lambda_{eq} = 0.3 + 6a \cdot (1 - \tanh(a - 0.5)) + 0.69 \cdot (\lambda_{a=1} - 3.52) \cdot a^{0.5} \cdot \left(1 + \tanh(a - \frac{0.89}{0.23})) + s \cdot (\lambda_{s=1} - \lambda_{a=1})\right) \quad (9)$$

$$a = {}^{p_{wv}}/_{p_{sat}} \quad (10)$$

$$\log p_{sat} = -2.1794 + 0.02953 \cdot (T - 273.15) - 9.1837 \cdot 10^{-5} \cdot (T - 273.15)^2 + 1.4454 \cdot 10^{-7} \cdot (T - 273.15)^3 \quad (11)$$

where ρ_l is the dry ionomer or membrane density (kg/m^3), EW is the equivalent weight of the membrane (kg/mol), γ_e and γ_c are the evaporation and condensation rate coefficients, λ_{eq}(mol H_2O/mol SO_3H) is the equilibrium water content, λ is the dissolved water content, $\lambda_{s=1} = 16.8$ and $\lambda_{a=1}$=9.2 are the water content for saturation and water activity equal to unity, p_{wv} is the water vapor partial pressure, a is the water activity and p_{sat} is the saturation pressure. The flux of liquid water at the interface between the GDL and the flow channel, f_{liq}, is assumed to be driven by the capillary pressure and the dynamic pressure in the gas channel [51]:

$$f_{liq} = \Theta \varepsilon s \cdot max\left[\left(p_c + \frac{1}{2}\rho V^2\right), 0\right] \quad (12)$$

where Θ is the coefficient of liquid water removal, and ρV^2 is the local dynamic head in the gas channel. The capillary pressure is obtained by solving equation (5) which is subsequently used to determine the liquid water saturation, s, using the Leverett function [52]:

$$p_c = \begin{cases} \sigma \cos\theta_c \sqrt{\frac{\varepsilon}{K}} J(1-s) & \theta_c < 90^\circ \\ \sigma \cos\theta_c \sqrt{\frac{\varepsilon}{K}} J(s) & \theta_c > 90^\circ \end{cases} \quad (13)$$

$$J(x) = ax - bx^2 + cx^3 \quad (14)$$

where σ (N/m) is the surface tension, θ_c(°) is the contact angle of the porous layer, a, b and c are user-specified Leverett function coefficients with the following default values: a=1.417, b=2.12, c=1.263.

The water produced at the catalyst surface is in a dissolved form. Depending on the gas phase saturation level, the dissolved water departs from the catalyst surface as a gas or as a liquid. For analysing the liquid water presence and the phase transfer between the liquid and water vapour (condensation/evaporation) the model incorporates the transport equations for the liquid phase in the GDLs, MPLs and in the gas channels. The exchange of liquid water between the gas channels and the gas diffusion layers is accounted for by the model in order to predict the pressure drop increase, using the following correlation:

$$\nabla \cdot (\rho_l \, u_l \, s) = \nabla \cdot (D_l \nabla s) \quad (15)$$

where D_l is the liquid water diffusion coefficient in the gas channels and u_l is the liquid velocity (assumed to be a part of the gas phase u_g). The liquid flux calculated from equation (12) is used as a boundary condition at the interfaces between the GDL and the channel for equation (15). For both fuel cell inlets the liquid saturation is set to be zero. When the equation (15) is solved, the channels are set automatically as porous zones and the Darcy law is applied taking into consideration the saturation:

$$\nabla p = -\mu \frac{1}{\alpha} v \tag{16}$$

where the resistance in the channels is given by [52]:

$$\frac{1}{\alpha} = 10^9 \cdot s^2 \left[\frac{1}{m^2}\right] \tag{17}$$

3. Numerical methodology

The ANSYS Fluent 2019 R1 software has been used in our computational fluid dynamics analysis [52]. In all the simulations, unless otherwise specified, a set of base case parameters and operating conditions have been used, see Table 4. The boundary conditions employed in the model are as follows. At the anode and cathode channel inlets: Dirichlet boundary conditions were prescribed, see Table 5 [47, 48]. Potentiostatic boundary conditions have been used to solve the solid phase potential, namely 0 V have been set for the anodic external wall and a value between 0 V and the open circuit voltage for the cathodic external wall. Further, the catalyst layer with the optimized microstructure parameters obtained previously [48] have been used in this study.

To obtain a converged solution, the governing equations are iteratively solved until the step between two consecutive residuals is less than 10^{-6} and the difference between the current produced in the anode CL and cathode CL is less than 10^{-4}. Parallel processing for ANSYS Fluent has been employed in all the simulations in order to reduce the time required for obtaining the polarization curves. In particular 32 processes shared on 2 workstations (two 8-core processors of 2.6 GHz and 64 GB of RAM each) were used. To obtain just 1 point on the polarization curve, using parallel processing, requires 2 hours of CPU time.

Table 4. The parameters used in the base case of the model [47, 48].

Parameter	Value	Unit
GDL/MPL/CL porosity (ε)	0.7/0.6/0.2	-
GDL/MPL/CL permeability (K)	$3\times10^{-12}/1\times10^{-12}/2\times10^{-13}$	m^2
Anodic reference exchange current density (j_a^{ref})	3000	A/m^2
Cathodic reference exchange current density (j_c^{ref})	0.3	A/m^2
H_2 molar concentration ($c_{H_2}^{ref}$)	54.6×10^{-3}	$kmol/m^3$
O_2 molar concentration ($c_{O_2}^{ref}$)	3.39×10^{-3}	$kmol/m^3$
Transfer coefficient at anode (α_a)	1	-
Transfer coefficient at cathode (α_c)	0.8	-
GDL/MPL/CL contact angle (θ_c)	110/130/95	^{o}
Anode/cathode specific surface area (ζ_c)	1.27×10^7	m_{Pt}^2/m_{CL}^3
Pt mass loading (m_{Pt})	0.2	mg/cm^2

Pt particle radius, (r_p)	2	nm
Resistance due to ionomer film (R_{ion})	100	S/m
Coefficient of liquid water removal (Θ)	5 x 10^{-5}	S/m
Open circuit voltage (V_{oc})	0.938	V
Membrane thickness	56	µm
GDL thickness	350	µm
MPL thickness	50	µm
Catalyst layer thickness	5.4	µm
Liquid water diffusion coefficient (D_{liq})	1×10^{-5}	m^2/s
Dry membrane density (ρ_i)	2000	kg/m^3
Equivalent weight of the membrane (EW)	1100	kg/kmol
Surface tension of water	0.0625	N/m

Table 5. The boundary conditions used in the model [47, 48].

Parameter	Value	Unit
Anodic mass flow rate at inlet	8×10^{-7}	kg/s
Cathodic mass flow rate at inlet	8×10^{-6}	kg/s
H_2 mass fraction at anode inlet	0.475	-
H_2O mass fraction for at anode inlet	0.525	-
O_2 mass fraction for at cathode inlet	0.242	-
H_2O mass fraction for at cathode inlet	0.0699	-
Relative humidity at anode/cathode inlets	56 %	-
Temperature at anode/cathode inlets	60	°C

The computational geometry displayed in Fig. 2 was created using the Gambit® 2.4.6 software and the mesh-independent solution geometry has about 1.1 million elements. The dimensions and the design of the 5 cm^2 active area fuel cell is the same as those of a real fuel cell. A 3-pass serpentine configuration for the flow field have been used for both the anode and cathode channels. The width and depth of each gas channel is 0.5 mm. A higher depth, i.e. 1.0 mm, is used for the region connecting the parallel channels of the serpentine pass, see Fig. 2. The bipolar plate is 22.5 mm × 22.5 mm in the x- and y – directions and its thickness is 1.5 mm [47].

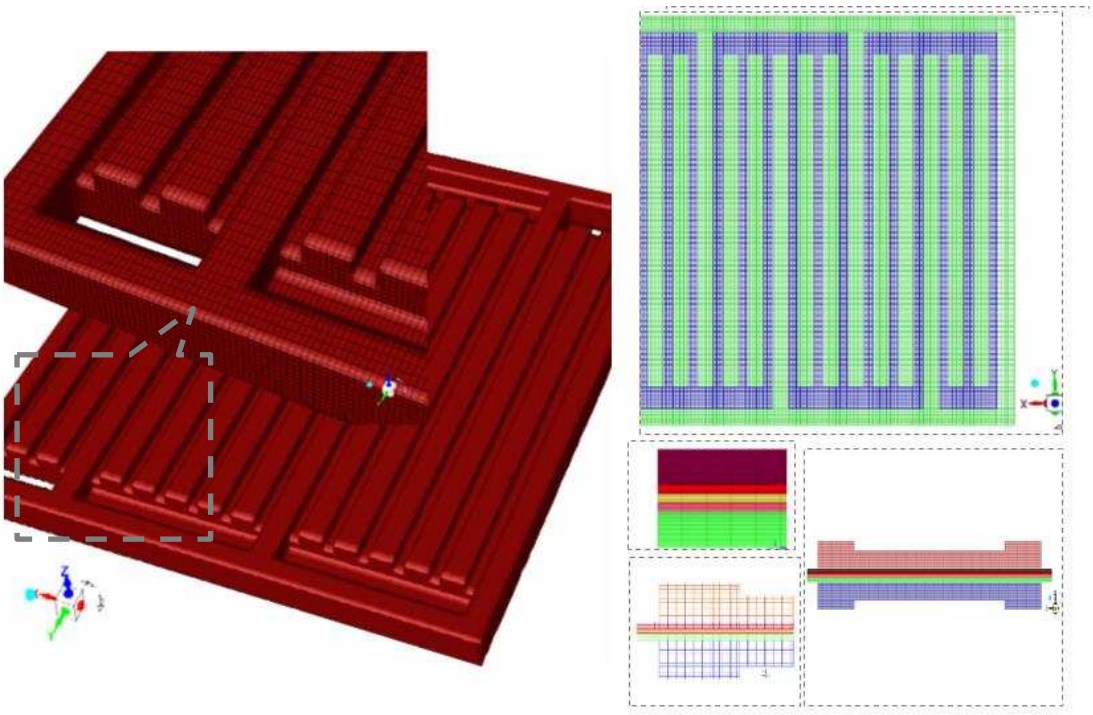

Fig. 2 – PEM fuel cell computational geometry and mesh.

4. Results and Discussions

4.1 Model Validation

A comparison between the numerical model results and experimental data from Marinoiu et al. [54] was performed for model validation. The 5 cm^2 PEM fuel cell used in the experiments was bought from ElectroChem and the runs were based on two configurations, namely with (using a novel in-house developed iodine doped graphene) and without MPLs and more details on the experimental procedures are available in [54]. It should be noted that the porosity of Toray GDL [58] used in the experiments was 0.6 and therefore this value was used in the model for validation. By comparing the polarization curves obtained experimentally and numerically using CFD simulations, it is found that there is good agreement between the two sets of results; see Fig. 3. However, there appears to be a discrepancy between the experimental and modelling data in the range 0.5-0.7 V, in particular for the case in which no MPLs were used; namely the model slightly overestimates the fuel cell performance in the ohmic losses-controlled region. This overestimation is probably due to the inability of the model to accurately capture the dehydration of the membrane that leads to a decrease in its proton conductivity. In the mass transport losses controlled region, more water is produced and consequently the ionic conductivity increases, leading to better agreement between the modelling and experimental results. An increase in the performance, of up to 12 %, in the ohmic and concentration losses dominated zones has been observed when the MPL was taken into consideration. This is mainly attributed to the enhanced electrical contact and better water management caused by the addition of the MPL layer [24]. [MI1]Materials used to develop the MPLs need to have excellent mechanical, thermal and electrical properties [24] and therefore iodine-doped graphene was used in developing our MPLs as this possess all the properties as evidenced by our findings [54] and those of [19, 22].

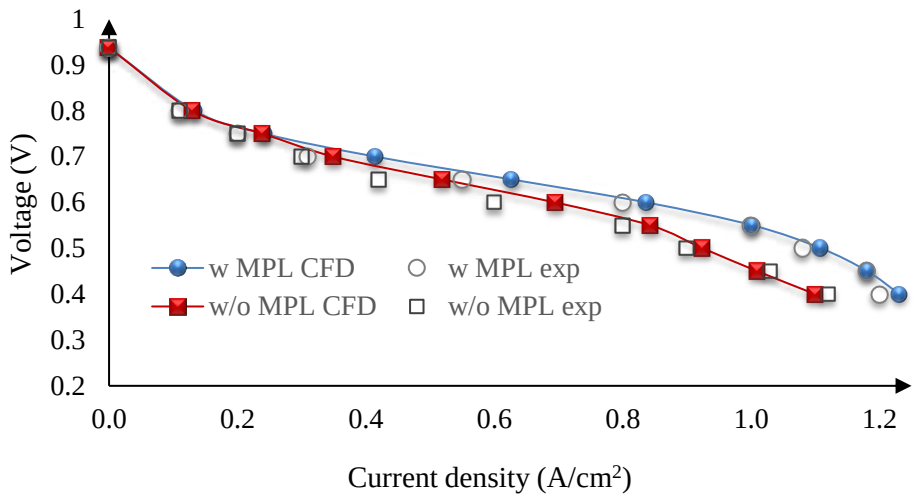

Fig. 3 – The experimental and simulated polarisation curves of the investigated fuel cell.

4.2 Effect of GDL microstructural properties

The GDL is typically made of highly porous and electrically conducting materials and it is an important layer .This is due to, as mentioned in the introduction of this paper, its multi-functional role in the fuel cell and to this end an optimized microstructure needs to be sought. The thickness, porosity, permeability and the contact resistance between the GDL and bipolar plate are some of the key parameters that have a considerable impact on the operation and performance of the PEM fuel cell. In addition to the manufacturing process that influences these parameters [21, 30, 32], compressive forces need to be applied to seal the single cell or the stack and this affects the microstructure of the porous layers (i.e. the GDLs, MPLs and the CLs) [31, 41-43]. The influence of these parameters on the performance is investigated and the results are presented in the form of polarisation curves and the local distribution of some of the key variables. Due to the fact that the normal operation of the PEM fuel cell is between 0.6 and 0.7 V, 0.6 V has been, unless otherwise specified, chosen as the operating voltage of the simulated fuel cell. Also, the base case conditions, listed in Table 4, have been used in our simulations unless otherwise specified.

4.2.1 Influence of the GDL thickness on the performance

The performance and water management of a fuel cell are influenced by the GDL thickness and these results are presented in Fig. 4 and Fig. 5. It can be noticed that decreasing the thickness of the GDL, from 350µm to 250µm,then an increase in the performance in the two zones of the polarization curves (the ohmic and concentration losses dominated zones) was achieved. This improvement with decreasing the GDL thickness, which could be as high as 10 %, is mainly due to the better rejection of liquid water as evidenced from the profile of the liquid water saturation at the interface between the cathode GDL and flow field plate, see Fig. 5. These results are in accordance with those found by Chun [13]. The effective rejection of liquid water from the MEA, especially at the cathode side, is essential to partially/completely clear the passages of the porous medium between the flow channel and catalyst layer to enable the reacting gases to reach the active sites in the catalyst layer. However, a thinner GDL thickness also reduces the mass transport resistance of the reacting/produced gases.

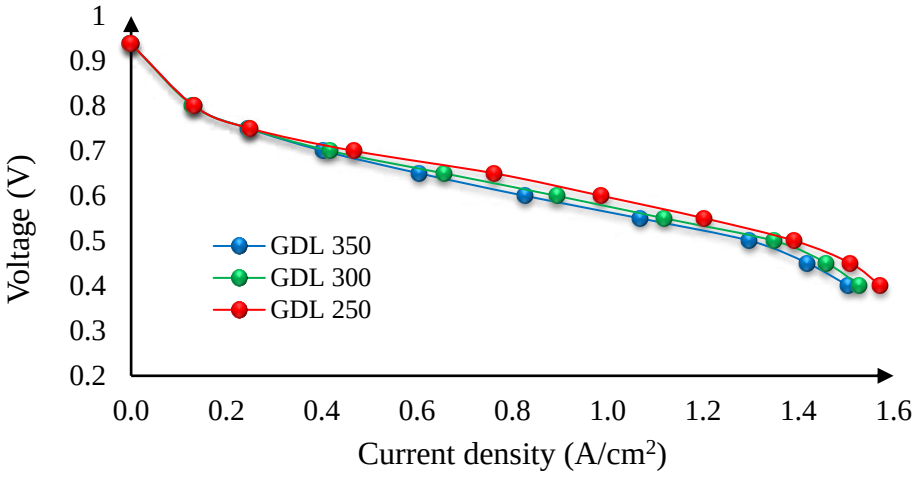

Fig. 4 - Polarization curves for different GDL thicknesses.

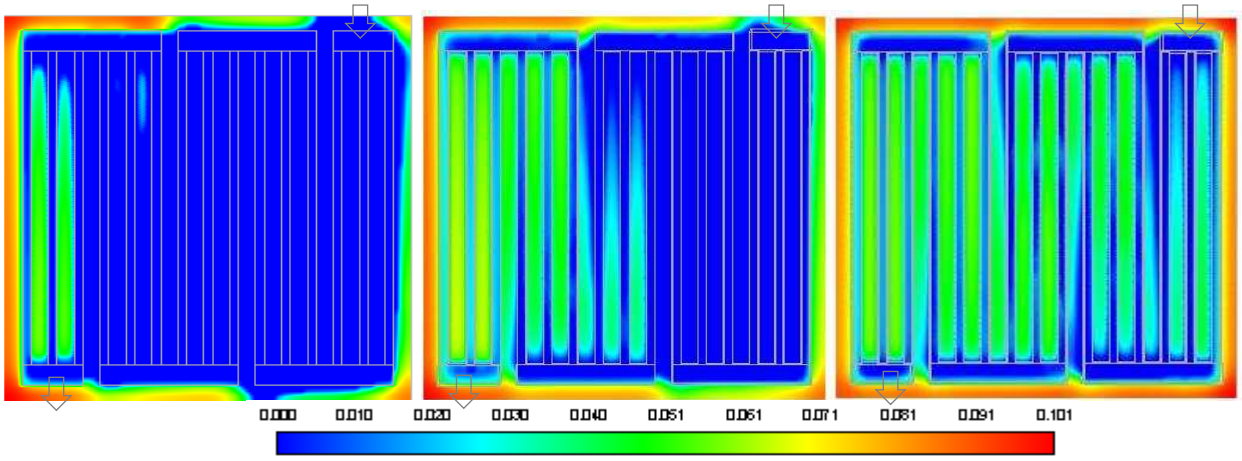

(a) (b) (c)

Fig. 5 – Liquid water saturation at the interface between the GDL and cathode channel for: (a) 350µm, (b) 300µm, and (c) 250 µm GDL thickness.

4.2.2 Influence of the porosity on the performance

Another important parameter that may significantly influence the performance is the GDL porosity which may vary between 0.3 and 0.8 as reported in [58-59]. The results displayed in Fig. 6 (a) reveal that the fuel cell performance improves with increasing the GDL porosity from 0.40 to 0.78 and many other studies have arrived at the same finding [26, 36-37, 58-62]. The profile of the oxygen mass fraction for different GDL porosity cases is presented in Fig. 6 (b)-(d). It may be clearly inferred that the consumption of oxygen is higher for the case with the largest GDL porosity (i.e. 0.78), see Fig. 6 (d). This translates into better fuel cell performance. The oxygen flow rate at the cathode inlet was 1.936×10^{-6} kg/s and at the cathode outlet was 1.13×10^{-6} and 1.57×10^{-6} kg/s for the GDL porosity cases of 0.78 and 0.40, respectively. This means that the consumption of oxygen has almost doubled when increasing the GDL porosity from 0.40 to 0.78. Fig. 7 displays the profile of the current density at the interface between the CL and MPL at 0.4V with different cathode GDL porosity (0.40, 0.60 and 0.78). As expected, due to the increased oxygen concentration (and subsequently increased reaction rate) at the catalyst layer, the highest current density values were those of the case with the highest GDL porosity. The gain in the reaction rate and the current density (due to the higher GDL porosity) leads to, due to the increasing Joule heating and other reversible and irreversible heat sources, an increase in the heat generated, as evidenced by the temperature profile at the interface between the MPL and the CL, see Fig. 8. Namely, the temperature, on average, increases by at least 10 °C when increasing the cathode GDL porosity from 0.4 to 0.78.

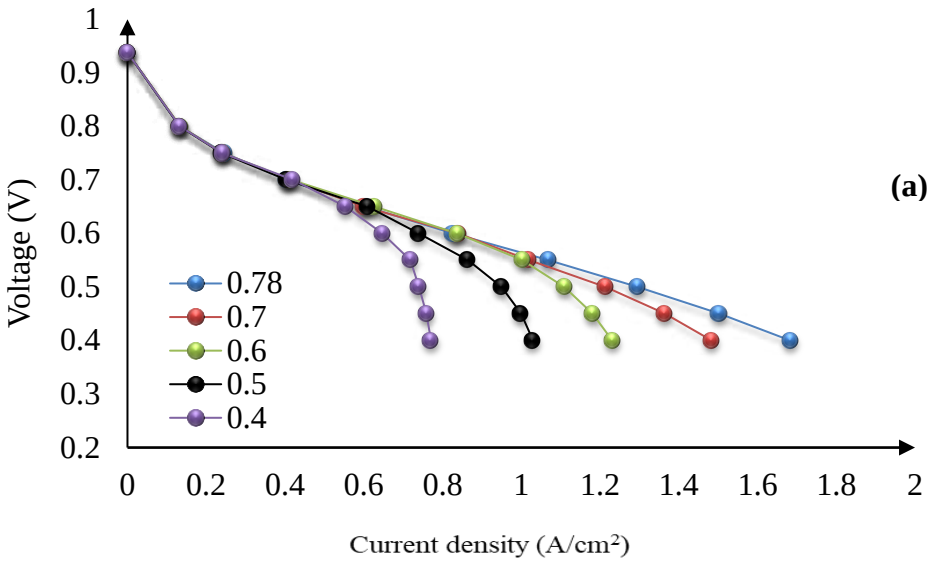

(a)

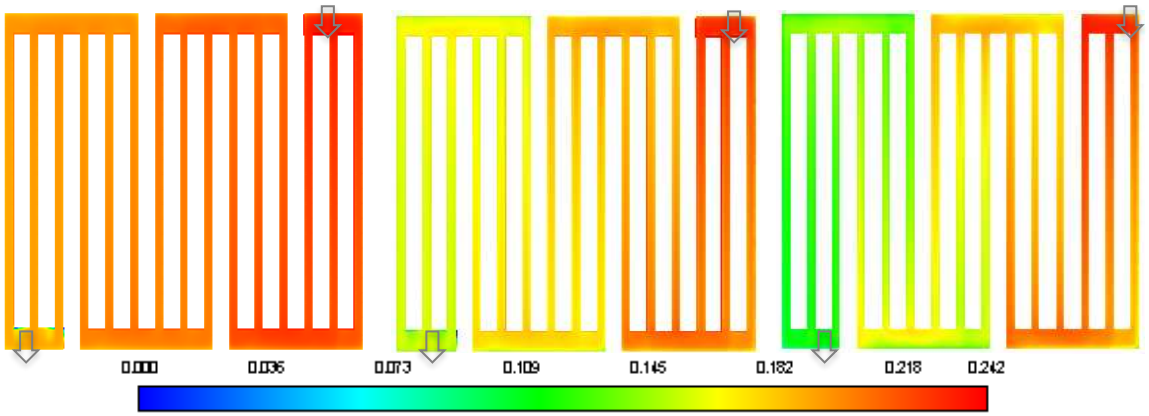

(b) **(c)** **(d)**

Fig. 6 (a) Polarization curves for different GDL porosities (ε); Oxygen mass fraction in the cathode channels for various cathode GDL porosity: (b) 0.4, (c) 0.6, and (d) 0.78.

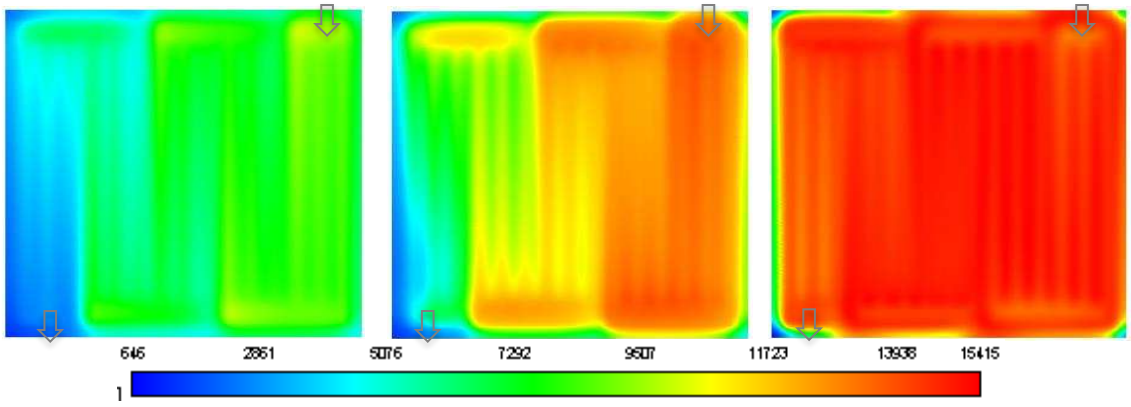

(a) **(b)** **(c)**

Fig. 7 – Profiles of current density at the interface between the CL and MPL at 0.4 V with different GDL porosity: (a) 0.4, (b) 0.6 and (c) 0.78.

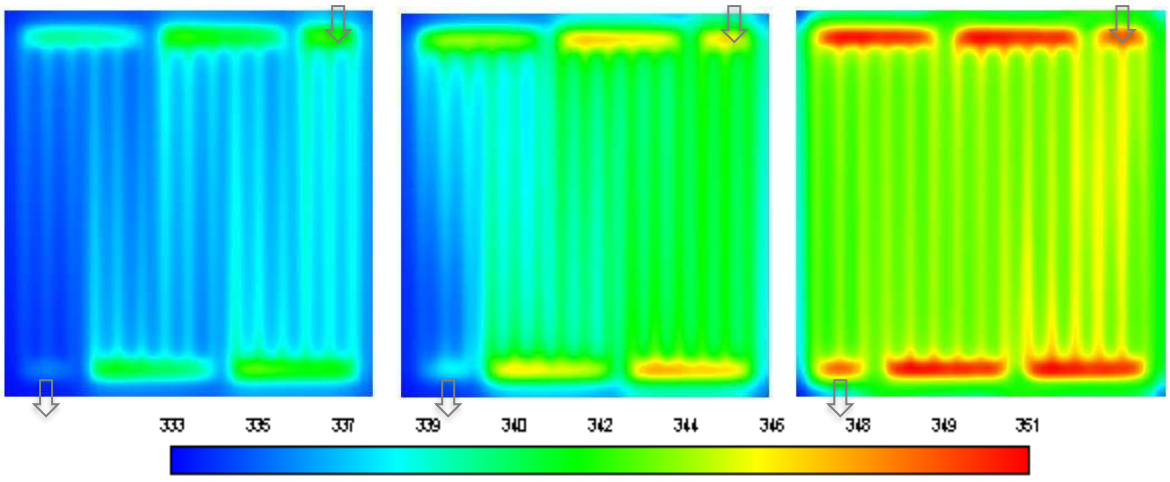

(a) **(b)** **(c)**

Fig. 8 – Temperature profiles at the interface between the CL and MPL at 0.4V with different cathode GDL porosity: 0.4, (b) 0.6 and (c) 0.78.

There are several studies that indicate graded GDL porosity enhances the water management and the mass transfer of gases inside the fuel cell [15-16, 44-45]. To numerically investigate this issue, a graded porosity for the cathode GDL has been implemented by developing a User Defined Function (UDF) in ANSYS Fluent. The UDF has been compiled and linked to the software in order to change the GDL porosity across its thickness. A gradual decrease of porosity from 0.7, near the channel, to 0.5 close to the MPL, has been implemented as a function of the GDL thickness. Fig. 9 shows that the fuel cell performance is better with the graded-porosity GDL, especially at the concentration losses controlled region. The case with constant porosity was taken to be the average of the extreme porosity values of the graded-porosity case, i.e. 0.6. The porosity of the MPL used in these simulations was chosen to be 0.3 and not 0.6 as in the base case conditions since we wanted to use different porosities for the GDL and MPL. The liquid water saturation at the interface between the cathode GDL and the flow field plate is displayed in Fig 9 (b)-(c) for the investigated cases. It is clear that the cathode GDL with graded-porosity uniformly rejects more water compared to that of the constant porosity and these results are consistent with those of Zhang et al. [5].

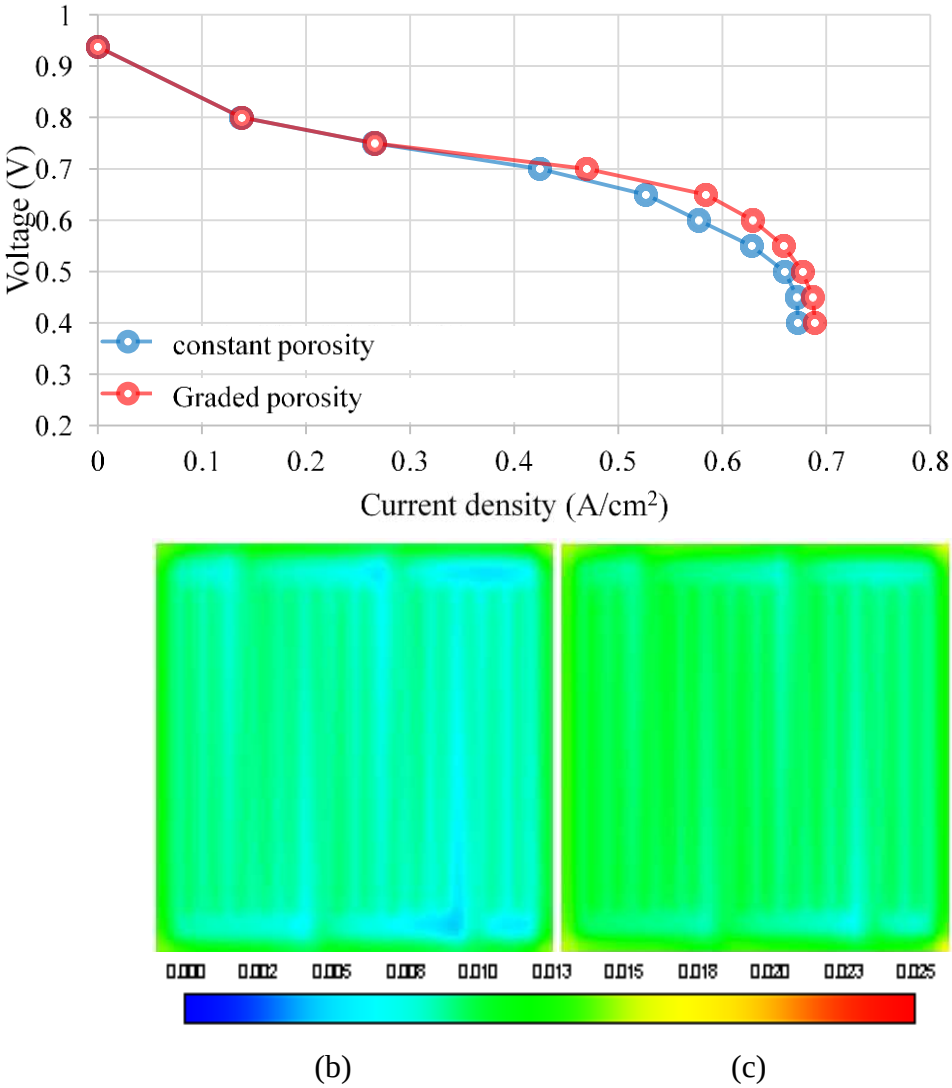

Fig. 9 (a) Polarization curves for different GDL porosities, Liquid water saturation (b) for constant porosity, and (c) for graded porosity

It should be noted that it is quite difficult to produce a GDL with a graded porosity and that is why most of the relevant investigations are modelling-based [5, 12, 15-16, 44-45]. Stimulated by the promising modelling results, production and test of in-house GDLs with a graded porosity is underway by the authors and will be reported in the future as soon as the relevant tests have been completed.

4.2.3 Influence of contact resistance (CR) between the BP and GDL

The numerical investigation carried out to determine the influence of the contact resistance between the GDL and BP reveals that a drop in the fuel cell performance is observed, especially in the ohmic losses and mass transport losses controlled regions, when incorporating different realistic values for the contact resistance of, say, 1×10^{-6} Ω·m^2, 4×10^{-6} Ω·m^2 and 7×10^{-6} Ω·m^2 between the GDL and BP, see Fig. 10. It could be seen from the latter figure that, at 0.4 V, the current density increases by 60% when decreasing the contact resistance from 7×10^{-6} to 1×10^{-6} Ω·m^2, signifying the critical influence of the contact resistance between the GDL and the bipolar plate on the PEMFC performance. Clearly, the contact resistance decreases with increasing clamping compression. However, the degree of compression must be optimised to ensure both good electrical contact and

oxygen supply to the catalyst layer in the regions located beneath the land of the bipolar plate. It must be mentioned that the highest GDL porosity has been used in these simulations (ε_{GDL}= 0.78) when considering the case without any compression applied, as is the case without any contact resistance.

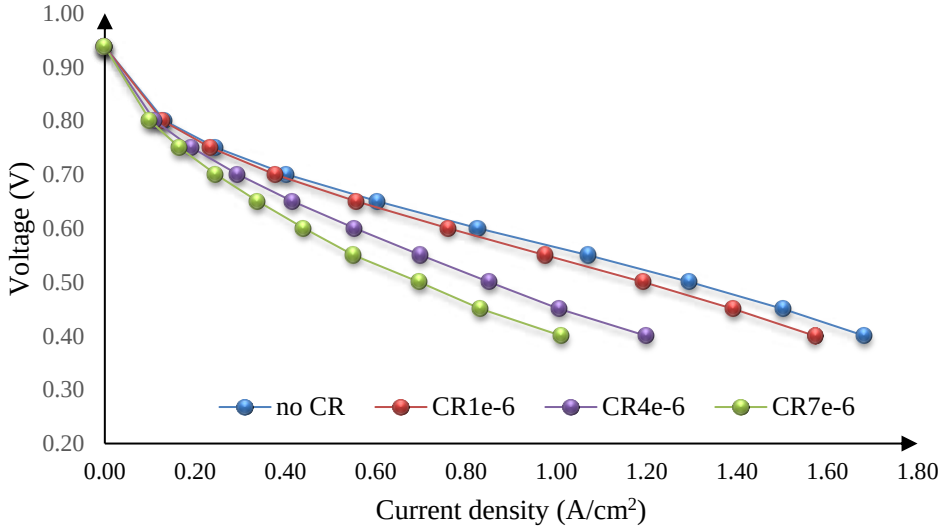

Fig. 10 - Polarization curves for the cases with and without CR (Ω·m^2) between the cathode GDL and BP.

4.3 Effect of MPL microstructural properties

The beneficial effect of the MPL addition on the performance of the fuel cell is mainly due to the improved electrical contact between the CL and GDL and the prevention of the fast dry-out of the membrane at low current densities and the flooding of the electrode at high current densities. In the next subsections, we investigate the effects of the presence of the MPL and its contact angle since these have a large influence on the water management and consequently on the fuel cell performance.

4.3.1 Effect of MPL addition to the GDL

The MPL added to the GDL typically enhances the overall performance of the PEM fuel cell, see Fig. 3. This is, as mentioned earlier, due to the improved water management induced by the MPL [19, 21-24]. The liquid water saturation profiles at the mid-thickness of the cathode and anode GDLs are displayed in Fig. 11 (a-d). It may be inferred from the figures that the added MPL forces the liquid water generated at the cathode to cross the membrane and reach the anode side. This could be justified by the presence of less liquid water at the cathode side (Fig. 11b) and more liquid water at the anode side (Fig. 11d) in the case when MPL is added. This must be compared with the profiles of the liquid water saturations at the cathode and anode sides in the absence of the MPL (Fig.11a and Fig. 11c). Further, Fig. 11(e-f) show the profile of the current density between the cathode GDL and the catalyst layer. It is clear that a higher and more uniform current density is obtained when MPL is added to the GDL.

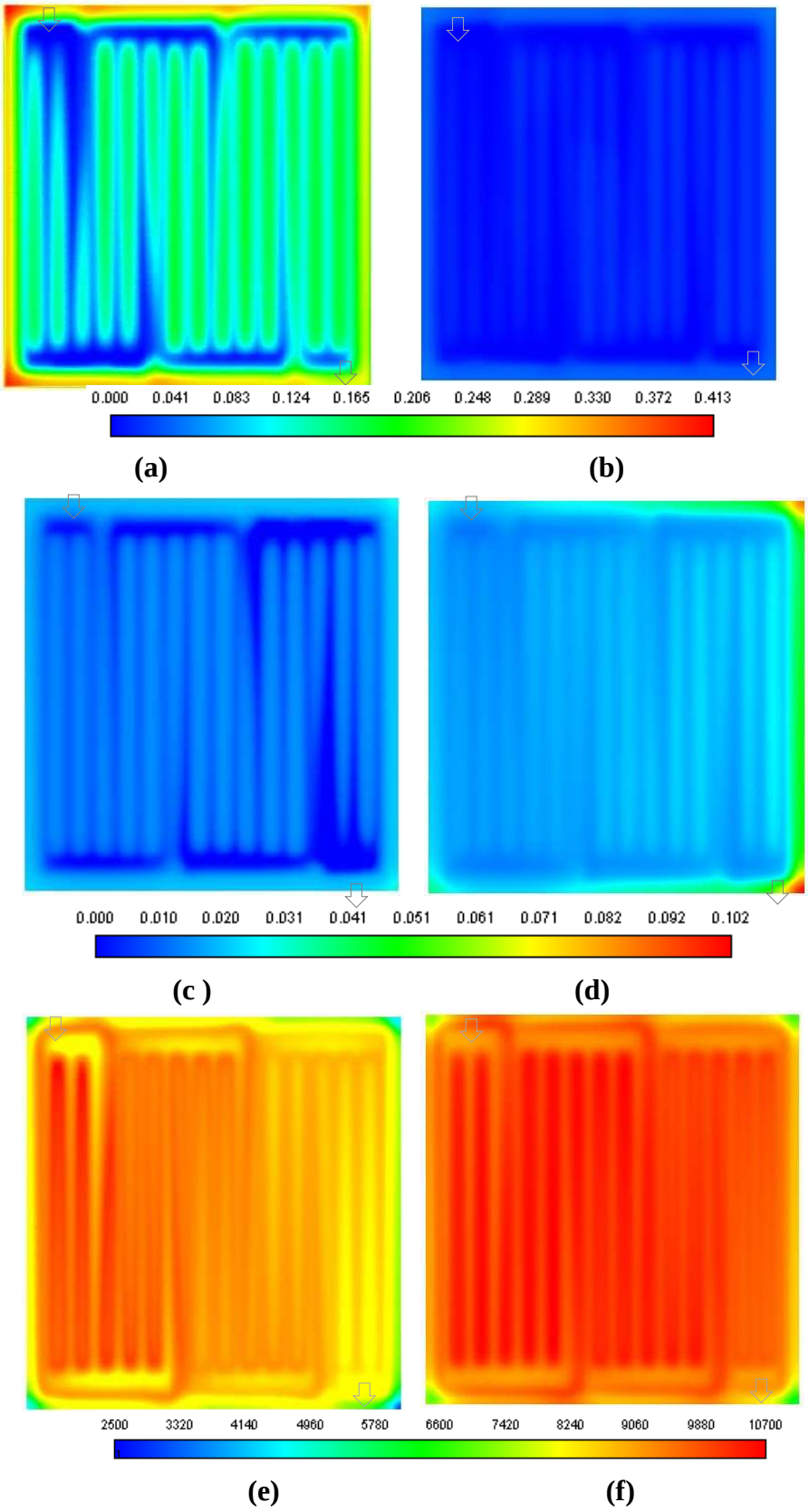

Fig. 11 – Profiles of liquid water saturation in the mid-thickness of the cathode GDL for the cases (a) without MPL and (b) with MPL. The liquid water saturation at the mid-thickness of the anode GDL for the cases (c) without MPL and (d) with MPL; and profiles of the current density at the interface between the cathode GDL and CL at 0.4 V potential difference for the cases (e) without MPL and (f) with MPL.

4.3.2 Influence of the MPL contact angle on the performance

The influence of the MPL contact angle was investigated and the respective polarization curves are displayed in Fig. 12. Typically the MPL has a hydrophobic nature, therefore three values, all more than 90°, have been chosen for the MPL contact angle in our study. By increasing the contact angle from 110 to 140°, a slight improvement in the performance was achieved and the results are consistent with Chun et al. [13]. The increase in the MPL hydrophobicity enhances slightly the water management, see Fig. 12. By taking into account the MPL, see Fig. 11 (a)-(d), a better water management was achieved. Further less liquid water in both sides (anode and cathode) of the simulated fuel cells with the MPL are obtained as compared with the case without MPL and these results are in accordance with Nam et al. [27] and Kandlikar et al. [34].

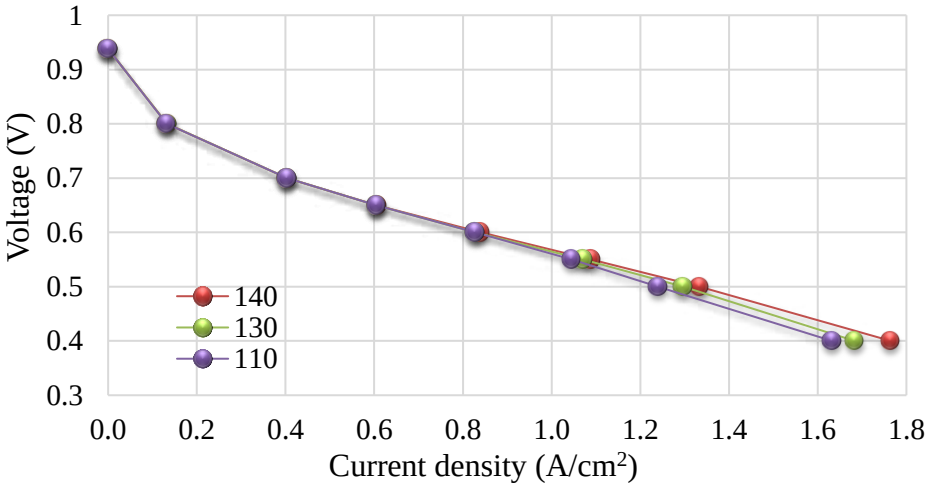

Fig. 12 - Polarization curve of the fuel cell as a function of the MPL contact angle.

5. Conclusions

A numerical model for a 5 cm² active area PEM fuel cell has been built to investigate the impact of some of the key parameters of the porous layers of the GDL and MPL on the performance. The outputs of the model, as polarisation curves, have been experimentally-validated for two cases: with/without MPLs. The main findings of the study are summarized as follows:

(i) The fuel cell performance slightly improves with increasing the GDL thickness and this is attributed to less resistance, to the transport of liquid water from the cathode catalyst layer to the flow channel, and to the flow of the reacting gas (i.e. oxygen gas in this case) from the flow channel to the catalyst layer.

(ii) A significant improvement in the fuel cell performance was achieved when increasing the porosity of the cathode GDL from 0.4 to 0.78 as the mass transport resistance of the reacting and product gases is significantly reduced.

(iii) The newly-introduced concept of graded-porosity GDL has been investigated. Ensuring more effective liquid water rejection, the fuel cell demonstrated a better performance with the graded-porosity GDL than with the conventional constant-porosity GDL.

(iv) The neglect of the electrical contact resistance between the GDL and bipolar plate results in an over-estimation of the fuel cell performance.

(v)The addition of the MPL was shown to have a positive influence on the fuel cell performance as it pushes liquid water to cross the membrane from the cathode side to the anode side, thus ensuring the humidification of the latter layer and subsequently enhancing the overall fuel cell

performance. Also, a realistic increase of the MPL contact angle has led to a slightly better performance of the fuel cell.

Acknowledgements

This work was supported by a grant of the Romanian Ministry of Research and Innovation, CCCDI - UEFISCDI, project number PN-III-P1-1.2-PCCDI-2017-0194/25 PCCDI within PNCDI III and by a project of the Romanian National Authority for Scientific Research & Innovation, within the Operational Competitiveness Program 2014-2020, Priority Axis 1, Action 1.1.4, contract 117/16.09.2016, RESTORE project, ID P_37_595.

References

[1] Omrani R, Shabani B. Review of gas diffusion layer for proton exchange membrane-based technologies with a focus on unitised regenerative fuel cells. Int J Hydrogen Energy 2019; 44(7): 3834-60.

[2] Wang J. Barriers of scaling-up fuel cells: Cost, durability and reliability. Energy 2015; 80: 509-21.

[3] Thepkaew J, Therdthianwong A, Therdthianwong S. Key parameters of active layers affecting proton exchange membrane (PEM) fuel cell performance. Energy 2008; 33:1794-800.

[4] Park S, Lee JW, Popov BN. A review of gas diffusion layer in PEM fuel cells: materials and designs. Int J Hydrogen Energy 2012; 37(7):5850–65.

[5] Zhang Y, Verma A, Pitchumani R. Optimum design of polymer electrolyte membrane fuel cell with graded porosity gas diffusion layer. Int. J Hydrogen Energy 2016; 41(20): 8412-26.

[6] Karpenko-Jereb L, Sternig C, Fink C, Theiler Andreas NV, Hacker V, Tatschl R. Theoretical study of an influence of the materials parameters on the performance of a polymer electrolyte fuel cell. J power sources K; 297: 329-43.

[7] Maynard HL, Meyers JP. Miniature fuel cells for portable power: Design considerations and challenges. J Vac Sci Technol B 2002; 20:1287-97.

[8] Manso AP, Marzo FF, Barranco J, Garikano X, Garmendia Mujika M. Influence of geometric parameters of the flow fields on the performance of a PEM fuel cell. A review. Int J Hydrogen Energy 2012; 37(20): 15256-87.

[9] Cerri I, Nagami T, Davies J, Mormiche C, Vecoven A, Hayden B. Innovative catalyst supports to address fuel cell stack durability, Int J Hydrogen Energy 2013; 38(1): 640-5.

[10] Berning T, Djilali N. A 3D, multiphase, multicomponent model of the cathode and anode of a PEM fuel cell. J Electrochem Soc 2003; 150: A1589 -98.

[11] Shimpalee S, Greenway S, Van Zee JW. The impact of channel path length on PEMFC flow-field design. J Power Sources 2006; 160: 398-406.

[12] Kong I, Jung A, Kim M. Investigations on the double gas diffusion backing layer for performance improvement of self- humidified proton exchange membrane fuel cells. Appl. Energy 2016; 176: 149-56.

[13] Chun JH, Park KT, Jo DH, Kim SG, Kim SH. Numerical modeling and experimental study of the influence of GDL properties on performance in a PEMFC. Int J Hydrogen Energy 2011; 36(2): 1837-45.

[14] Xing L, Wang Y, Das PK, Scott K, Shi. Homogenization of current density of PEM fuel cells by in-plane graded distributions of platinum loading and GDL porosity. Chem Eng Sci 2018; 192: 699-713.

[15] Chen F, Chang M-H, Hsieh P-T. Two-phase transport in the cathode gas diffusion layer of PEM fuel cell with a gradient in porosity. Int J Hydrogen Energy 2008; 33(10): 2525-29.

[16] Huang YX, Cheng CH, Wang XD, Jang JY. Effects of porosity gradient in gas diffusion layers on performance of proton exchange membrane fuel cells. Energy 2010; 35(12):4786–94.
[17] Shimpalee S, Beuscher U, Van Zee JW. Analysis of GDL flooding effects on PEMFC performance. Electrochem Acta 2007; 52: 6748-54.
[18] Pauchet J, Prat M, Schott P, Pulloor Kuttanikkad S. Performance loss of proton exchange membrane fuel cell due to hydrophobicity loss in gas diffusion layer: Analysis by multiscale approach combining pore network and performance modelling. Int J Hydrogen Energy 2012; 37:1628-41.
[19] Nam JH, Lee K-J, Hwang G-S, Kim C-J, Kaviany M. Microporous layer for water morphology control in PEMFC. Int J Heat Mass Transf 2009; 52(11-12):2779-91.
[20] Sadiq Al-Baghdadi M, Shahad Al-Janabi H. Parametric and optimization study of a PEM fuel cell performance using three dimensional computational fluid dynamics model J Renewable Energy 2007; 32: 1077-101.
[21] Park SB, Kim S, Park Y, Oh M-H. Fabrication of GDL microporous layer using PVDF for PEMFCs, J Phys: Conf Ser 2009; 165(1): 012046
[22] Nishiyama, E.; Murahashi, T. Water transport characteristics in the gas diffusion media of PEMFC – Role of the microporous layer. J. Power Sources, 2011, 196(4), 1847-1854
[23] Weber AZ, Newman J. Effects of microporous layers in polymer electrolyte fuel cells, J Electrochem Soc 2005; 152(4): A677-88.
[24] Tseng C-J, Lo S-K. Effects of microstructure characteristics of gas diffusion layer and microporous layer on the performance of PEMFC. Energ Convers Manage 2010. 51(4): 677-84.
[25] Steinbach AJ, Allen JS, Borup RL, Hussey DS, Jacobson DL, Komlev A, Kwong A, MacDonald J, Mukundan R, Pejsa MJ, Roos M, Santamaria AD, Sieracki JM, Spernjak D, Zenyuk IV, Weber AZ. Anode-Design Strategies for Improved Performance of Polymer-Electrolyte Fuel Cells with Ultra-Thin Electrodes. Joule 2018; 2(7): 1297-312.
[26] Lee H-K, Park J-H, Kim D-Y, Lee T-H. A study on the characteristics of the diffusion layer thickness and porosity of the PEMFC, J Power Sources 2004; 131(1–2): 200-6.
[27] Nam JH, Kaviany M. Effective diffusivity and water-saturation distribution in single- and two-layer PEMFC diffusion medium. Int J Heat Mass Tran 2003; 46: 4595–611.
[28] Karpenko-Jereb L, Sternig C, Fink C, Hacker V, Theiler A, Tatschl R. Theoretical study of the influence of material parameters on the performance of a polymer electrolyte fuel cell. J Power Sources 2015; 297: 329-43.
[29] Ahmed DH, Sung HJ, Bae J. Effect of GDL permeability on water and thermal management in PEMFCs — I. Isotropic and anisotropic permeability. Int J Hydrogen Energy 2008; 33(14):3767-85.
[30] Ismail MS, Hughes KJ, Ingham DB, Ma L, Pourkashanian M. Effect of PTFE loading of gas diffusion layers on the performance of proton exchange membrane fuel cells running at high-efficiency operating conditions Int J Energy Res 2013; 37: 1592-9.
[31] Tanaka S, Bradfield W. Numerical and experimentally study of the effects of the electrical resistance and diffusivity under clamping pressure on the performance of a metallic gas-diffusion layer in polymer electrolyte fuel cells. J. Power Sources 2016; 330: 273-84.
[32] Orogbemi OM, Ingham DB, Ismail MS, Hughes KJ, Ma L, Pourkashanian M. Through-plane gas permeability of gas diffusion layers and microporous layer: effects of carbon loading and sintering. J Energy Inst 2018; 91(2):270-8.
[33] Das PK, Grippin A, Kwong A, Weber AZ. Liquid-Water-Droplet Adhesion-Force Measurements on Fresh and Aged Fuel-Cell Gas-Diffusion Layers. J Electrochem Soc 2012; 159(5): B489-96.
[34] Kandlikar SG, Garofalo ML, Lu Z. Water Management in A PEMFC: Water transport mechanism and material degradation in Gas Diffusion Layers. Fuel Cells 2011; 6:814-23.

[35] Fadzillah DM, Rosli MI, Talib MZM, Kamarudin SK, Daud WRW. Review on microstructure modelling of a gas diffusion layer for proton exchange membrane fuel cells. Renewable and Sustainable Energy Reviews 2017; 77: 1001-9.
[36] Inoue G, Yoshimoto T, Matsukuma Y, Minemoto M. Development of simulated gas diffusion layer of polymer electrolyte fuel cells and evaluation of its structure. J Power Sources 2008; 175(1): 145-58.
[37] Larbi B, Alimi W, Chouikh R, Guizani A. Effect of porosity and pressure on the PEM fuel cell performance, Int J Hydrogen Energy 2013; 38: 8542-9.
[38] Hiramitsu Y, Sato H, Hori M. Prevention of the water flooding by micronizing the pore structure of gas diffusion layer for polymer electrolyte fuel cell, J Power Sources 2010; 195(17): 5543-9.
[39] Pierre JS, Wilkinson D, Knights S. Relationships between water management contamination and lifetime degradation in PEMFC. J New Mater Electrochem Syst 2000; 3:99–106.
[40] Knights SD, Colbow KM, St-Pierre J, Wilkinson DP. Aging mechanisms and lifetime of PEFC and DMFC. J Power Sources 2004; 127(1–2): 127-34.
[41] Shi Z, Wang X, Guessous L. Effect of compression on the water management of a Proton Exchange Membrane Fuel Cell with different gas diffusion layers, J Fuel Cell Sci Tech 2010; 7: 021012-1-7.
[42] Zhou P, Wu CW, Ma GJ. Influence of clamping force on the performance of PEMFCs, J Power Sources 2007; 163: 874-81.
[43] Su ZY, Liu CT, Chang HP, Li CH, Huang KJ, Sui PC. A numerical investigation of the effects of compression force on PEM fuel cell performance. J Power Sources 2008; 183(1): 182-92.
[44] Tang H, Wang S, Pan M, Yuan R. Porosity-graded micro-porous layers for polymer electrolyte membrane fuel cells. J Power Sources 2007; 166: 41–6.
[45] Chun JH, Jo DH, Kim SG, Park SH, Lee CH, Lee ES, Jyoung J-Y, Kim SH. Development of a porosity-graded micro porous layer using thermal expandable graphite for proton exchange membrane fuel cells, Renew Energy 2013; 58: 28-33.
[46] Andrei RD, Marinoiu A, Bucura F, Zaharioiu A, Niculescu V, Sisu C, Carcadea E. Synthesis via electrospinning of electrospun polyacrylonitrile fibers – preliminary results, Progress of Cryogenics and Isotopes Separation 2018; 21(2):81-90.
[47] Carcadea E, Varlam M, Marinoiu A, Raceanu M, Ismail MS, Ingham DB. Influence of catalyst structure on PEM fuel cell performance – A numerical investigation, Int J Hydrogen Energy 2019: 44(25):12829-41.
[48] Carcadea E, Varlam M, Ingham DB, Ismail MI, Patularu L, Marinoiu A, Schitea D. The effects of cathode flow channel size and operating conditions on PEM fuel performance: A CFD modelling study and experimental demonstration. Int J Energy Res 2018; 42(8):2789-804 .
[49] Barbir F. PEM Fuel Cell: Theory and Practice. 2nd ed. Amsterdam; Boston: Elsevier Academic Press; 2012.
[50] Um S, Wang CY, Chen KS. Computational Fluid Dynamics Modeling of Proton Exchange Membrane Fuel Cells. J Electrochem Soc 2000; 147(12) 4485-93.
[51] Scholz H. "Modellierung und Untersuchung des Wärme- und Stofftransports und von Flutungsphänomenen in Niedertemperatur-PEM-Brennstoffzellen". PhD Thesis. 2015.
[52] ANSYS. Multiphysics help, www.ansys.com
[53] Springer TE, Zawodzinski TA, Gottesfeld S. Polymer Electrolyte Fuel Cell Model. J Electrochem Soc 1991; 138: 2334–42.
[54] Marinoiu A, Varlam M, Carcadea E, Raceanu M, Soare A, Stefanescu I. A Class of High Performance Electrocatalysts for Oxygen Reduction Reaction of Fuel Cells, using Iodine Doped Graphene. Mater Today: Proc 2018; 5: 15915–22.
[55] Jang J-H, Yan W-M, Shih C-C. Effects of the gas diffusion-layer parameters on cell performance of PEM fuel cells. J Power Sources 2006; 161: 323–32.

[56] Toghyani S, Moradi Nafchi F, Afshari E, Hasanpour K, Baniasadi E, Atyabi SA. Thermal and electrochemical performance analysis of a proton exchange membrane fuel cell under assembly pressure on gas diffusion layer. Int J Hydrogen Energy 2018; 43(9): 4534-45.
[57] Sunden B, Faghri M. Transport phenomena in Fuel Cells. Series: Developments in Heat Transfer, 19:175-208. WIT Press; 2005.
[58] El-kharouf A, Mason TJ, Brett DJL, Pollet BG. Ex-situ characterisation of gas diffusion layers for proton exchange membrane fuel cells. J Power Sources 2012; 218: 393-404.
[59] Zhou Y, Jiao K, Du Q, Yin y, Li X. Gas diffusion layer deformation and its effect on the transport characteristics and performance of proton exchange membrane fuel cell. Int J Hydrogen Energy 2013; 38: 12891-903.
[60] LaManna M, Kandlikar SG. Determination of effective water vapor diffusion coefficient in pemfc gas diffusion layers. Int J Hydrogen Energy 2011; 36(8): 5021-9.
[61] Flückiger R, Freunberger SA, Kramer D, Wokaun A, Scherer GG, Büch FN. Anisotropic, effective diffusivity of porous gas diffusion layer materials for PEFC. Electrochim Acta 2008; 54: 551-9.
[62] Taspinar R, Litster S, Kumbur EC. A computational study to investigate the effects of the bipolar plate and gas diffusion layer interface in polymer electrolyte fuel cells. Int J Hydrogen Energy 2015; 40(22): 7124-34.